

Morphometric Analysis of Hippocampal Shape in Mild Cognitive Impairment: An Imaging Genetics Study

Li Shen and Andrew J. Saykin

Center for Neuroimaging, Dept. of Radiology
Center for Computational Biology & Bioinformatics
Indiana University School of Medicine
950 W Walnut St, R2 E124, Indianapolis, IN 46202
Email: shenli@iupui.edu, asaykin@iupui.edu

Moo K. Chung

Biostatistics & Medical Informatics
Univ. of Wisconsin Madison
1300 University Ave.,
Madison, WI 53706
Email: mkchung@wisc.edu

Heng Huang

Computer Science & Engineering
Univ. of Texas at Arlington
Box 19015, 416 Yates St.,
Arlington, TX 76019
Email: heng@uta.edu

Abstract—A computational framework is presented for surface based morphometry to localize shape changes between groups of 3D objects. It employs the spherical harmonic (SPHARM) method for surface modeling and random field theory (RFT) for statistical inference. Several new components are introduced to overcome previous limitations: (1) a general linear model is used to facilitate controlling for covariates; (2) a new SPHARM registration method SHREC is proposed to better align SPHARM models; and (3) an estimated smoothness is used in RFT-based analysis to obtain more accurate results. This framework is applied in a mild cognitive impairment (MCI) study to examine hippocampal shape changes related to diagnostic and genetic conditions. Several interesting findings from our analyses suggest combining imaging phenotypes and genetic profiles has the potential to elucidate biological pathways for better understanding MCI and Alzheimer’s disease.

I. INTRODUCTION

Statistical morphometric analysis is used in biomedical imaging to study various structures of interest, and aims to identify morphometric abnormalities associated with a particular condition in order to aid diagnosis and treatment. We have previously developed a surface-based morphometry (SBM) framework and applied it to a neuroimaging genetics study for relating hippocampal shape changes to certain conditions in mild cognitive impairment (MCI) [18], [19]. In this work, we introduce several novel components into our SBM framework in order to achieve more accurate and more effective results. We use the same MCI data to demonstrate the effectiveness of our new framework.

MCI [14] is characterized by memory complaints and impairment in the absence of dementia and confers a high risk for Alzheimer’s disease (AD). Brain imaging methods for identifying medial temporal morphological abnormalities [4], [16] in circuits required for learning and memory have been studied for early diagnosis and treatment of MCI and AD. The connection between genotype and imaging phenotype has yet to be established, which can help identify possible genetic risk factors for MCI and AD.

Although Apolipoprotein E (APOE) appears related to subtle cognitive and neuroimaging changes [20], late-onset AD is a complex disorder that undoubtedly involves many genes and polymorphisms. For example, the Interleukin-6 (IL-6) gene

is a proinflammatory cytokine involved in neuronal signaling that appears to reduce hippocampal neurogenesis [12], and the single-nucleotide polymorphism (SNP) of IL-6 in the -174 promoter region appears to modulate the reduction of medial temporal volume and gray matter concentration in older adults with memory decline [15].

In this study, we perform morphometric analysis aiming at a global and local quantitative representation of hippocampal shape changes related to certain conditions in MCI. One condition to evaluate is the interaction between morphometric changes of the hippocampus and the IL-6 -174 SNP. We classify this as an imaging genetics study, where imaging genetics [9] refers to the study of genetic variation using imaging measures as phenotypes.

To achieve the above goal, we develop an improved SBM framework that can localize regionally specific shape changes between groups of 3D objects. Our framework incorporates spherical harmonic (SPHARM) method [2] for surface modeling, heat kernel smoothing [5] for increasing surface signal to noise ratio, and random field theory (RFT) [5], [21] for statistical inference directly on the surface. This new framework overcomes several limitations of our previous method [18], [19], which are described below.

Our previous method employs t-test for statistical inference and cannot exclude the effect of any covariate. In this work, we perform statistical analysis using general linear model (GLM), which allows us to obtain more accurate results by removing effects of covariates. For example, to identify hippocampal shape changes in MCI, we often need to remove the age effect. To relate shape changes to IL-6 SNP, the effect of APOE-ε4 needs to be excluded.

Our previous method uses the first order ellipsoid (FOE) for registering SPHARM models, which may not work in general. In this work, we present a general registration approach called SHREC, based on minimizing the distance between the corresponding SPHARM models [17]. We demonstrate that SHREC can not only create more accurate registration than the FOE approach but also do it efficiently.

Smoothness estimation is a key step in RFT-based analysis [21]. The smoothness measure used in our previous study is predicted from heat diffusion equations [5]. A recent study [8]

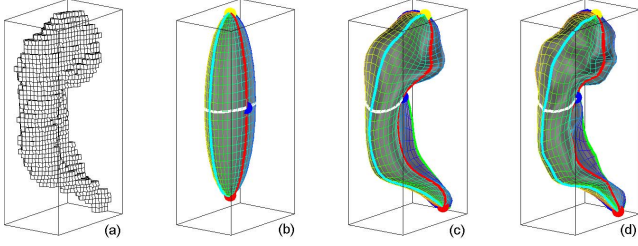


Fig. 1. Sample voxel object surface (a) and its SPHARM reconstructions (b-d) using coefficients up to degrees 1, 8 and 15.

shows that the accuracy of such a prediction is limited. In this work, we use the approach proposed in [8] to estimate the smoothness for more accurate results.

II. SURFACE MODELING AND REGISTRATION

A. SPHARM Description

The spherical harmonic (SPHARM) description [2] is used for modeling all the hippocampal surfaces. Its first step is to create a continuous and uniform mapping from the object surface to the surface of a unit sphere. It is formulated as a constrained optimization problem with the goals of topology and area preservation and distortion minimization. The result is a bijective mapping between each point \mathbf{v} on a surface and a pair of spherical coordinates θ and ϕ : $\mathbf{v}(\theta, \phi) = (x(\theta, \phi), y(\theta, \phi), z(\theta, \phi))^T$.

Now the object surface can be expanded into a complete set of spherical harmonic basis functions Y_l^m , where Y_l^m denotes the spherical harmonic of degree l and order m . The expansion takes the form:

$$\mathbf{v}(\theta, \phi) = \sum_{l=0}^{\infty} \sum_{m=-l}^l \mathbf{c}_l^m Y_l^m(\theta, \phi),$$

where $\mathbf{c}_l^m = (c_{xl}^m, c_{yl}^m, c_{zl}^m)^T$. The coefficients \mathbf{c}_l^m up to a user-desired degree can be estimated by solving a set of linear equations in a least squares fashion. The object surface can be reconstructed using these coefficients, and using more coefficients leads to a more detailed reconstruction.

Figure 1 shows a sample surface and its SPHARM reconstructions using coefficients up to degrees 1, 8 and 15. The degree one reconstruction is always an ellipsoid for any SPHARM model. We call it the *first order ellipsoid* (FOE). Here we superimpose a colored mesh onto a SPHARM reconstruction to show its underlying parameterization. On the mesh, the yellow, red, and blue dots indicate the north pole $(0, 0)$, the south pole $(0, \pi)$, and the crossing point of the zero meridian and the equator $(0, \pi/2)$, respectively.

B. SPHARM Registration

SPHARM registration aims to register all the models into a common reference system to facilitate shape comparison. It creates a normalized set of SPHARM coefficients, which are comparable across objects, to form a shape descriptor (*i.e.*, excluding translation, rotation, and scaling). *Scaling*

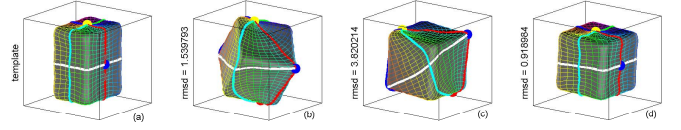


Fig. 2. SHREC idea: (a) template, (b) FOE aligned object, (c) roughly aligned in object space, (d) aligned in parameter space.

invariance can be achieved by adjusting the coefficients so that a certain volume is normalized. In our experiments, we employ three scaling schemes HP, BV, and IC, which normalize for hippocampal volume (HP), brain tissue volume (BV), and intracranial volume (IC), respectively. Ignoring the degree 0 coefficient results in *translation invariance*.

To achieve *rotation invariance*, traditional SPHARM methods try to align FOE to a canonical position [2]. This approach works only if the FOE is a real ellipsoid but not an ellipsoid of revolution or a sphere. In the latter case, some undesired result may happen (e.g., Figure 2(a,b)). To bridge this gap, we present a SPHARM registration method by minimizing the root mean squared distance (RMSD) between two models instead of aligning the FOEs and by incorporating the widely used iterative closest point (ICP) strategy [1]. We call our algorithm *SHREC*, standing for *SPHARM RE*gistration with *ICP* [17]. The key idea is to perform the following two steps alternately until some stopping criterion is met: (1) creating surface correspondence, and (2) minimizing the distance between the corresponding surface parts. The correspondence between SPHARM models is implied by the underlying parameterization: two points with the same parameter pair (θ, ϕ) on two surfaces are defined to be a corresponding pair. Thus, in order to create an ideal correspondence, we can first align two models in the object space (Figure 2(c)) and then rotate the parameter net of one model to best match the other's (Figure 2(d)).

1) *Rotating Parameterization*: A naive solution for rotating the parameterization of a SPHARM model is to recalculate the SPHARM coefficients using the rotated parameterization. However, this requires to solve three linear systems and is time-consuming. To accelerate the process, we use a rotational property in the harmonic theory and rotate SPHARM coefficients without recalculating the SPHARM expansion.

Let $\mathbf{v}(\theta, \phi) = \sum_{l=0}^{\infty} \sum_{m=-l}^l \mathbf{c}_l^m Y_l^m(\theta, \phi)$ be a SPHARM parametric surface. After rotating the parameter net on the surface in Euler angles $(\alpha\beta\gamma)$, the new coefficients $c_l^m(\alpha\beta\gamma)$ can be calculated as follows [3], [10], [13]

$$c_l^m(\alpha\beta\gamma) = \sum_{n=-l}^l D_{mn}^l(\alpha\beta\gamma) c_l^n \quad (1)$$

where

$$D_{mn}^l(\alpha\beta\gamma) = e^{-i\gamma n} d_{mn}^l(\beta) e^{-i\alpha m},$$

$$d_{mn}^l(\beta) = \sum_{t=\max(0, n-m)}^{\min(l+n, l-m)} (-1)^t$$

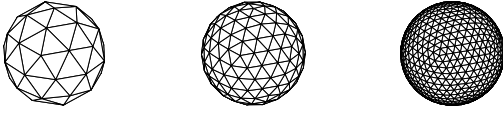


Fig. 3. Icosahedral samples at levels 1-3.

$$\begin{aligned} & \times \frac{\sqrt{(l+n)!(l-n)!(l+m)!(l-m)!}}{(l+n-t)!(l-m-t)!(t+m-n)!t!} \\ & \times \left(\cos \frac{\beta}{2} \right)^{(2l+n-m-2t)} \left(\sin \frac{\beta}{2} \right)^{(2t+m-n)}. \end{aligned}$$

This rotational property was previously used in [3], [13] to simulate rotations of a spherical function by rotating only the harmonic expansion coefficients. In SPHARM representation, we use three spherical functions (*i.e.*, $x(\theta, \phi)$, $y(\theta, \phi)$, $z(\theta, \phi)$) to describe a 3D object so that we can deal with intrusions and protrusions, and model any simply connected object. SPHARM separates the geometry information in the object space from the parameterization in the parameter space. If we rotate all three functions by $(\alpha\beta\gamma)$, only the parameterization is rotated in the parameter space and the object stays the same in the object space.

2) *Registration of Parameterization*: We first focus on how to create surface correspondence between two models that are roughly aligned in the object space. Since the underlying parameterization defines the correspondence between different SPHARM surfaces, our task is to rotate the parameterization of one model to best match the other's. The goodness of the match is measured by the root mean squared distance (RMSD) between two models. RMSD can be calculated directly from SPHARM coefficients. Let S_1 and S_2 be two SPHARM surfaces, where their SPHARM coefficients are formed by $\mathbf{c}_{1,l}^m$ and $\mathbf{c}_{2,l}^m$, respectively, for $0 \leq l \leq L_{max}$ and $-l \leq m \leq l$. The RMSD between S_1 and S_2 can be calculated as follows [7]:

$$\text{RMSD} = \sqrt{\frac{1}{4\pi} \sum_{l=0}^{L_{max}} \sum_{m=-l}^l \|\mathbf{c}_{1,l}^m - \mathbf{c}_{2,l}^m\|^2}. \quad (2)$$

We employ a sampling-based strategy that fixes one parameterization and rotates the other to optimize the surface correspondence by minimizing the RMSD defined in Eq. 2. The rotation space can be sampled nearly uniformly using icosahedron subdivisions (Figure 3). This assigns rotation angles to β and γ . Let n be the number of icosahedral samples. The expansion coefficients are then rotated through $(0\beta\gamma)$ and then by \sqrt{n} equal steps in α using Eq. 1, evaluating the RMSD at each orientation. The result is the best orientation that minimizes the RMSD. Conceptually, each icosahedral vertex is rotated onto the north pole, followed by further rotations about the north-south axis; this gives a nearly uniform coverage of the parameter space.

Clearly, the registration accuracy of this approach mostly depends on its sampling resolution. More samples usually indicate a better result but more running time. In order to achieve good accuracy and also keep the running time under

control, we propose a hierarchical sampling scheme instead of simple icosahedral sampling. Our idea is to begin our search at low resolution and find top K promising candidate orientations. Then we perform local searches at high resolution for these candidates to update our candidate set. The process can be repeated for higher and higher resolutions until the result is satisfactory or there is no more change in the top K list. This approach is described in Algorithm 1.

Algorithm 1 Hierarchical registration of parameterization.

```

1:  $i:=1$ 
2: repeat
3:   Create icosahedral samples at level  $i$  for  $\beta$ 's and  $\gamma$ 's
4:   Let  $n$  be the number of icosahedral samples
5:   Create  $\sqrt{n}$  equally spaced samples in  $[0, 2\pi)$  for  $\alpha$ 's
6:   if  $i=1$  then
7:     Rotate parameterization using each  $(\alpha\beta\gamma)$ , and keep
       the top  $K$  candidates that minimize RMSD
8:   else
9:     Keep only local icosahedral samples for  $\beta$ 's &  $\gamma$ 's
10:    Rotate parameterization for each top  $K$  candidate
       using each  $(\alpha\beta\gamma)$ , and create a new set of top  $K$ 
       candidates for the next iteration
11:   $i:=i+1$ 
12: until No more changes in top  $K$  list or satisfactory result
       obtained
13: Return the best result in top  $K$  list

```

Similar two-step approaches for registering spherical harmonic expansions have been proposed in [10], [13]. At low resolution, [10] uses a random generator to create rotation samples. One disadvantage of this approach is that different runs often derive different results. For [13], icosahedral samples are also used at low resolution. At high resolution, both [10] and [13] use a quasi-Newton function minimization method to identify a nearby local minimum. In this work, our hierarchical sampling method suggests a unified scheme using icosahedral samples at both low and high resolutions, is very easy to implement, and works very well.

3) *SPHARM Registration using ICP*: A simple method to use ICP [1] is as follows. We can first create surface samples and then use ICP to align these points together in the object space. Here ICP removes both translational and rotational effects. Then we can register the parameterization to establish the surface correspondence. This approach is simple, can roughly align SPHARM models together, but does not derive optimized results.

To optimize an initial alignment, we can divide the registration into two stages, one for the parameter space and one for the object space. Now, we can alternately improve the alignment in the object space and the alignment in the parameter space. This is basically the ICP idea. The alignment in the parameter space can be improved by running Algorithm 1. To improve the alignment in the object space, since an initial surface correspondence has already be created,

we can simply create corresponding surface samples between SPHARM models and use a quaternion-based algorithm to align two corresponding point sets together in a least squares sense [1]. For convenience, we call this quaternion-based algorithm as CPS (*i.e.*, aligning corresponding point sets). To start the above iterative procedure, we need an initial registration, which can be done by ICP or FOE. Algorithm 2 summarizes the above ideas and presents SHREC.

Algorithm 2 SHREC: SPHARM registration with ICP

- 1: Set up initial alignment using FOE or ICP
 - 2: **repeat**
 - 3: Run CPS to align models in the object space
 - 4: Run Algorithm 1 to align the parameter nets
 - 5: **until** No more changes in the parameter space
-

III. STATISTICAL MORPHOMETRIC ANALYSIS

A. Surface Signal Processing

To perform statistical shape analysis, we need to extract signals or variables on the surface to describe a shape. We define the mean of all the healthy controls as our template, \mathbf{x}_t , which can be thought of as an average and normal shape. For an individual shape \mathbf{x} , we can use its deformation field $\delta(\mathbf{x}) = \mathbf{x} - \mathbf{x}_t$ relative to the template \mathbf{x}_t to describe it. Note that, for each surface landmark, there are three related elements (corresponding to x, y, z coordinates) in $\delta(\mathbf{x})$.

We employ the NML and FLD schemes in [18] to define the surface signal. In NML, we look at the deformation component along the surface normal direction. In FLD, we examine the most “discriminative” direction, since our goal is to detect shape changes between groups. We use Fisher’s linear discriminant [6] to find the direction; and use the deformation component along this direction as surface signal.

To increase the signal-to-noise ratio (SNR), we employ heat kernel smoothing (HKS) [5] that generalizes Gaussian kernel smoothing to arbitrary Riemannian manifolds. The smoothness (*i.e.*, full-width-half-max (FWHM) size of the heat kernel) can be predicted from heat diffusion equations. A recent study [8] shows that the accuracy of such a prediction is limited, which suggests a smoothness estimation step is necessary even for RFT-based analysis using HKS.

The smoothness is related to the covariance matrix of the partial derivatives of the error field. In practice, it is calculated using the residual values from the statistical analysis. In this work, we estimate the smoothness FWHM_{surf} from the residual error of each subject after fitting it to the linear model and we use the following approach proposed in [8].

$$\text{FWHM}_{surf} = dv \cdot \sqrt{\frac{-2 \ln 2}{\ln\left(1 - \frac{\text{var}(ds)}{2 \text{var}(s)}\right)}} \quad (3)$$

where dv is the average inter-neighbor distance, $\text{var}(ds)$ is the variance of inter-neighbor differences, and $\text{var}(s)$ is the overall variance of the values at each vertex. We calculate a single

smoothness for the entire data set by averaging all individual FWHMs.

B. General Linear Model

As noted before, in our previous study [18], [19], we employ t-test for statistical inference, which cannot exclude the effect of any covariate. However, in a typical neuroimaging study, it is often necessary to remove the effect of certain covariates (*e.g.*, age, APOE-e4). To achieve this goal, we consider the following general linear models (GLMs):

$$\begin{aligned} \text{signal} &= \phi_1 + \phi_2 \cdot \text{age} + \psi_1 \cdot \text{group} + \epsilon \\ \text{signal} &= \phi_1 + \phi_2 \cdot \text{age} + \phi_3 \cdot \text{apoe-e4} + \psi_1 \cdot \text{group} + \epsilon \end{aligned}$$

To make a general form, let $Z = (z_1, \dots, z_k)$ to be nuisance variables such as age and APOE-e4 and $X = (x_1, \dots, x_p)$ to be the variable of interest such as group. Then we have GLM in the following form

$$y = Z\Phi + X\Psi + \epsilon \quad (4)$$

where $\Phi = (\phi_1, \dots, \phi_k)^T$ and $\Psi = (\psi_1, \dots, \psi_p)^T$. We assume the usual zero mean Gaussian noise. Then we test if the group is significant, that is,

$$\begin{aligned} H_0 : \quad &\Psi = 0 \quad \text{for all } y \in \partial\Omega \\ \text{vs.} \\ H_1 : \quad &\Psi \neq 0 \quad \text{for some } y \in \partial\Omega. \end{aligned}$$

The fit of model is measured by the residual sum of squares or the sum of the squared errors (SSE):

$$\begin{aligned} \text{SSE}_0 &= \sum_{i=1}^{m+n} (y_i - Z_i \hat{\Phi}_0)^2 \\ \text{SSE}_1 &= \sum_{i=1}^{m+n} (y_i - Z_i \hat{\Phi}_1 - X_i \hat{\Psi}_1)^2 \end{aligned}$$

where $\hat{\Phi}_0, \hat{\Phi}_1, \hat{\Psi}_1$ are the least squares estimators of the parameters and Z_i and X_i are data for the i -th subject. Then under H_0 ,

$$F = \frac{(\text{SSE}_0 - \text{SSE}_1)/p}{\text{SSE}_0/(m+n-p-k)} \sim F_{p, m+n-p-k} \quad (5)$$

The larger the F value, it is more unlikely to accept H_0 . For testing group difference controlling for age, $k = 2$ and $p = 1$, while for testing group difference controlling for both age and apoe-e4, $k = 3$ and $p = 1$.

C. Random Field Theory

We use random field theory (RFT) [5], [21] for multiple comparison corrections on the surface. The application of RFT involves two steps: (1) estimate the smoothness of the surface data, which we have discussed before; (2) use the smoothness values in the appropriate RFT equation to determine statistical thresholds that control the familywise error rate (FWER) and provide corrected P values for the result.

Here we give RFT equations for an F field. For a T field, see [5] for its equations. If $F(x)$ is a smooth F field, the

	Age (mean±std)	Education (mean±std)	Sex (M,F)	IL-6 (CC,CG,GG)
HC	70.6±5.0	16.6±2.7	12, 28	10, 13, 17
CC	72.8±6.1	16.5±2.7	16, 23	7, 25, 7
MCI	72.2±6.9	16.4±3.2	21, 16	10, 18, 9
ALL	71.8±6.1	16.6±2.7	49, 67	27, 56, 33

TABLE I
PARTICIPANT CHARACTERISTICS

corrected P value for correcting multiple comparisons over all vertices on the hippocampal surface $\partial\Omega$ is given by

$$P(\sup_{x \in \partial\Omega} F(x) > h) \approx \sum_{d=0}^2 \mu_d(\partial\Omega) \rho_d(h) \quad (6)$$

where μ_d are the d dimensional Minkowski functionals of $\partial\Omega$ and ρ_d are the d dimensional Euler characteristic (EC) density. The Minkowski functionals are $\mu_0 = 2, \mu_1 = 0, \mu_2 = \text{area}(\partial\Omega)/2$, the half area of the template hippocampus $\partial\Omega$. For an F random field with α and β ($\alpha = p$ and $\beta = m + n - p - k$ for the above case) degrees of freedom, the EC-densities are given by

$$\begin{aligned} \rho_0(h) &= \int_h^\infty \frac{\Gamma(\frac{\alpha+\beta-2}{2})}{\Gamma(\frac{\alpha}{2})\Gamma(\frac{\beta}{2})} \alpha \left(\frac{\alpha x}{\beta}\right)^{\frac{\alpha-2}{2}} \left(1 + \frac{\alpha x}{\beta}\right)^{-\frac{(\alpha+\beta)}{2}} dx \\ \rho_2(h) &= \frac{\lambda}{2\pi} \frac{\Gamma(\frac{\alpha+\beta+2}{2})}{\Gamma(\frac{\alpha}{2})\Gamma(\frac{\beta}{2})} \left(\frac{\alpha h}{\beta}\right)^{\frac{\alpha-2}{2}} \left(1 + \frac{\alpha h}{\beta}\right)^{-\frac{(\alpha+\beta-2)}{2}} \\ &\quad \times \left[(\beta-1) \frac{\alpha h}{\beta} - (\alpha-1) \right] \end{aligned}$$

where $\lambda = 1/(2\sigma^2)$ measures the smoothness of fields. In terms of FWHM of a smoothing kernel, the smoothness of field is given as $\lambda = 4 \ln 2 / \text{FWHM}^2$. As noted before, the FWHM is estimated using an approach described in [8].

IV. EXPERIMENTAL RESULTS

A. Data Set

Participants include healthy controls (HC, $n = 40$), euthymic older adults with cognitive complaints (CC, $n = 39$) but intact neuropsychological performance, and patients with amnesic MCI ($n = 37$). Table I shows several participant characteristics [16]. MRI scan data are acquired on a 1.5 Tesla GE scanner as a T1-weighted SPGR coronal series. The hippocampi are segmented using the BRAINS software package [11]. A 3D binary image is reconstructed from each set of 2D hippocampal segmentation results.

All hippocampi are expanded using SPHARM coefficients up to degree 15; thus, each one is described by $(15+1)^2 * 3 = 768$ coefficients. The tests are performed on a Dell Workstation PWS670 with a Xeon 3GHz CPU and 1GB of RAM, running WinXP and Matlab 7. Different scaling schemes are tested in our experiments: normalizing for hippocampal volume (HP), brain tissue volume (BV), and intracranial volume (IC). For each scaling scheme, we create a template that is the mean of the controls.

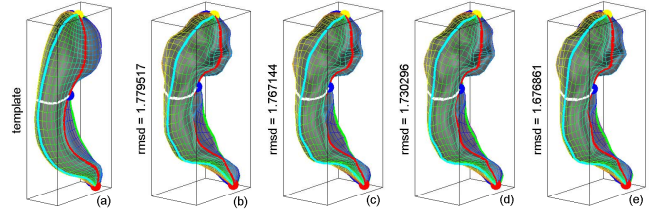


Fig. 4. Sample SHREC result: (a) template, (b) FOE aligned object, (c) after CPS, (d) after Alg. 1, (e) after another CPS and Alg. 1.

	RMSD (before)	RMSD (after)	Time (sec.)
left	1.788 ± 0.408	1.753 ± 0.384	60.0 ± 23.3
right	1.854 ± 0.446	1.815 ± 0.416	60.0 ± 21.3

TABLE II
SHREC RESULTS ON ALIGNING 116 HIPPOCAMPAL PAIRS

B. Registration using SHREC

As noted before, FOE registration cannot work when the FOE is not a real ellipsoid but a ellipsoid of revolution or a sphere. FOE registration has also a symmetry problem and may create multiple results. In these cases, SHREC can be used to align things together and remove the ambiguity. Using SHREC, we can also improve the result of FOE registration. Figure 4 shows a sample result. In (a), the template is shown. In (b), the result of FOE registration is shown. In (c), the result of aligning (b) to (a) by running CPS is shown. In (d), the result of aligning (c) to (a) by running Algorithm 1 is shown. In (e), the final result is shown. We see that SHREC improves the RMSD effectively and progressively from (b) to (e) through its iterative procedures.

In another experiment, we run SHREC on 116 pairs of left and right hippocampi that are already aligned using FOE registration. The templates to which SHREC registers hippocampi are the mean left and right hippocampi. Table II shows simple statistics of the results in terms of registration accuracy in RMSD and the running time. The statistics include mean and standard deviation shown as (mean ± std). The second column shows the RMSD to the template before running SHREC; and the third column shows the RMSD after running SHREC. The improvement over the FOE registration is obvious. The last column shows the running time. We can see that SHREC is very efficient, considering that all the experiments are performed on a common desktop.

C. Group Analyses

In the first experiment, we perform pairwise group analyses among HC, CC and MCI using NRM signals and the IC scaling scheme. Figure 5(a) shows the t-values mapped onto the mean right hippocampus, while Figure 6(a) shows the f-values derived from general linear model (GLM) while controlling for age. Using random field theory (RFT), corrected p values can be calculated for both t-maps and f-maps, which are converted to $-\log(\text{corrected p-values})$ and then shown in Figure 5(b) and Figure 6(b). These analyses indicate that statistically

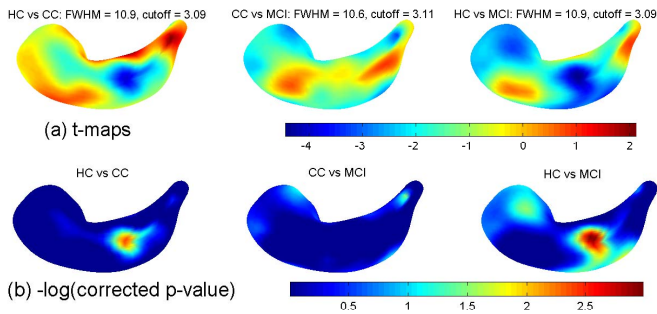


Fig. 5. Results of t-test for NRM signals on right hippocampi (IC scaling): (a) t-maps; (b) $-\log(\text{corrected } p\text{ values})$.

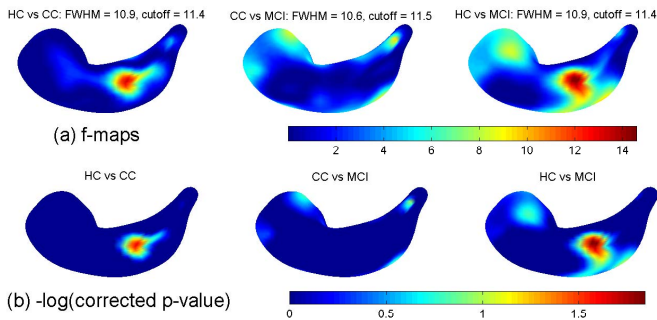


Fig. 6. Results of f-test for NRM signals on right hippocampi (controlling for age): (a) f-maps; (b) $-\log(\text{corrected } p\text{ values})$.

significant regions of shape changes mostly appear between HC and MCI. The CC group shows a more intermediate pattern.

Figure 7 and Figure 8 show significant regions after thresholding at 95% confidence level for t-maps and f-maps, respectively. Here we show the results using both NRM signals (see (a)) and FLD signals (see (b)). After excluding the age effect, GLM gives more conservative results than t-test in terms of significant shape changes. Another observation is that FLD signals are more sensitive than NRM ones on localizing the shape changes, which matches our intuition.

Note that significant regions on a t-map can be either blue (large negative t-values) or red (large positive t-values), while those on an f-map can only be red because there is no negative f-values. In all the experiments, we use FWHM = 8mm for heat kernel smoothing. The estimated FWHMs are printed in most of the figures and they have a range between 6.7 (Figure 9) and 11.1 (Figure 10). For each of Figures 7-10, two rows correspond to two different views.

Due to the space limit, we can only summarize our findings and demonstrate a few results here. A more detailed report will be written in an extended version of this work. In pairwise group analyses among HC, CC and MCI, substantial shape changes can be detected on right hippocampi using GLM controlling for age under BV or IC scaling scheme between HC and MCI, but neither between HC and CC nor between CC and MCI. See Figures 5-8 for example.

In most of our experiments, t-test is very optimistic and of-

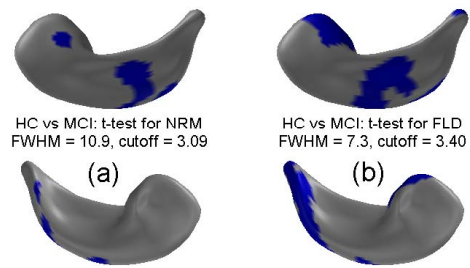


Fig. 7. Significant regions (95% confidence level) of t-test for HC versus MCI on right hippocampi: (a) NRM signals; (b) FLD signals. Two rows correspond to two different views.

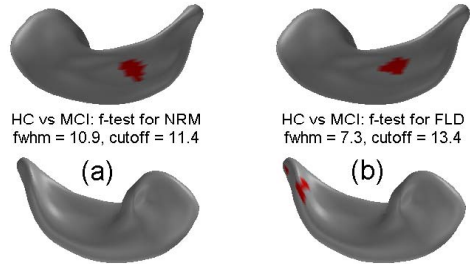


Fig. 8. Significant regions (95% confidence level) of f-test for HC versus MCI on right hippocampi (controlling for age): (a) NRM signals; (b) FLD signals.

ten reports many shape changes. We feel that, after controlling age, APOE-e4, or both, GLM gives more reliable results and contains less false positives. Thus, in the rest, we only report our GLM results using FLD signals.

In the second experiment, we perform pairwise group analyses among different IL-6 polymorphisms: C/C, C/G, and G/G. Using f-test, shape changes can be identified on the left hippocampi between G/G and C/G (Figure 9(a)), and on the right hippocampi between G/G and C/C (Figure 9(b)). Between C/C and C/G, there is no significant changes on either left or right hippocampi.

In the third experiment, we perform group analyses for HC versus each IL-6 -174 SNP genotype (C/C, C/G, G/G) for the diagnostic group MCI. Significant changes can be detected only between HC and homozygous MCIs (i.e., C/C and G/G) on right hippocampi (Figure 10).

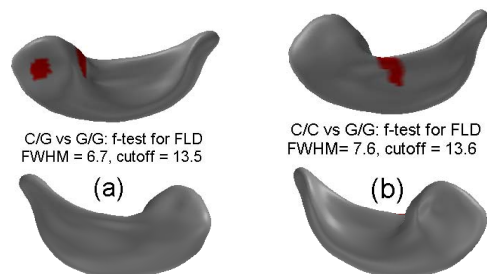


Fig. 9. f-test for G/G versus C/G or C/C (controlling for age and APOE-e4, HP scaling): (a) G/G vs C/G on left hippocampi; (b) G/G vs C/C on right hippocampi.

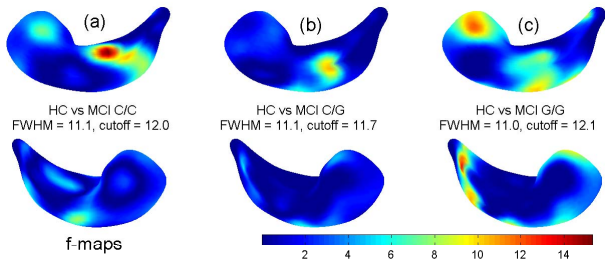


Fig. 10. f-test for HC vs each MCI genotype on right hippocampi (controlling for age and APOE-e4, IC scaling): (a) HC vs MCI C/C, (b) HC vs MCI C/G., (c) HC vs MCI G/G.

V. CONCLUSIONS

We have performed a mild cognitive impairment (MCI) study to examine hippocampal shape changes related to certain conditions including the diagnostic group and the IL-6 -174 SNP. In our analysis, we have developed an improved surface based morphometry (SBM) framework that can localize regionally specific shape changes between groups of 3D objects. Our framework employs the spherical harmonic (SPHARM) method for surface modeling and random field theory (RFT) for statistical inference. To overcome several limitations of our previous method, this new framework incorporates the following new components: (1) f-test using GLM is used for statistical inference to remove effects of related covariates such as age, APOE-e4, or both; (2) a new SPHARM registration method SHREC is proposed to better align SPHARM models; and (3) an estimated smoothness is used in RFT-based analysis to obtain more accurate results.

Our result shows that substantial shape changes mostly appear between CN and MCI, and the CC group showed a more intermediate pattern. Among different IL-6 genotypes, we can detect shape changes between G/G and either of C/C and C/G, while no shape change appears between C/C and C/G. If we compare HC with each genotype in the MCI group, shape changes can be detected only between HC and homozygous MCIs (i.e., C/C and G/G). These findings suggest that brain imaging phenotypes, genetic profiles, and cognitive measures, in combination, have the potential to elucidate the biological pathways related to memory processes and therapeutic response in MCI and AD. An interesting future topic could be to investigate a systems biology approach for understanding the genetic architecture of MCI and AD by examining more neuroimaging phenotypes related to candidate pathways composed of ensembles of genomically distributed but functionally related genes.

ACKNOWLEDGMENT

Funded, in part, by grants from the US NIH (NIA R01 AG19771; U54 EB005149) and the Alzheimer's Association. Part of the work was done while Li Shen was with the CIS department at UMass Dartmouth.

REFERENCES

- [1] P. J. Besl and N. D. McKay. A method for registration of 3-D shapes. *IEEE Trans. on PAMI*, 14(2):239–256, 1992.
- [2] C. Brechbühler, G. Gerig, and O. Kubler. Parametrization of closed surfaces for 3D shape description. *Computer Vision and Image Understanding*, 61(2):154–170, 1995.
- [3] G. Burel and H. Hennocq. Determination of the orientation of 3D objects using spherical harmonics. *Graphical Models and Image Processing*, 57(5):400–408, 1995.
- [4] R. Chen and E. H. Herskovits. Network analysis of mild cognitive impairment. *NeuroImage*, 29:1252–1259, 2006.
- [5] M. K. Chung, S. Robbins, K. M. Dalton, et al. Cortical thickness analysis in autism via heat kernel smoothing. *NeuroImage*, 25:1256–1265, 2005.
- [6] R. O. Duda, P. E. Hart, and D. G. Stork. *Pattern Classification (2nd ed.)*. Wiley, New York, NY, 2000.
- [7] G. Gerig, M. Styner, et al. Shape analysis of brain ventricles using SPHARM. In *IEEE MMBIA*, pages 171–178, 2001.
- [8] D. J. Hagler, A. P. Saygin, and M. I. Sereno. Smoothing and cluster thresholding for cortical surface-based group analysis of fMRI data. *NeuroImage*, 33:1093–1103, 2006.
- [9] A. R. Hariri, E. M. Drabant, and D. R. Weinberger. Imaging genetics: Perspectives from studies of genetically driven variation in serotonin function and corticolimbic affective processing. *Biological Psychiatry*, 59:888–897, 2006.
- [10] H. Huang, L. Shen, et al. Surface alignment of 3D spherical harmonic models: Application to cardiac MRI analysis. In *MICCAI'2005, LNCS 3749*, pages 67–74, 2005.
- [11] Iowa MHCRC Image Processing Lab. *Brains Software*. <http://www.psychiatry.uiowa.edu/ipl/>.
- [12] G. Kempermann and G. Kronenberg. Depressed new neurons—adult hippocampal neurogenesis and a cellular plasticity hypothesis of major depression. *Biological Psychiatry*, 54:499–503, 2003.
- [13] D. W. Ritchie and G. J. Kemp. Fast computation, rotation, and comparison of low resolution spherical harmonic molecular surfaces. *Journal of Comp. Chem.*, 20:383–395, 1999.
- [14] A. J. Saykin and H. A. Wishart. Mild cognitive impairment: conceptual issues and structural and functional brain correlates. *Seminars in Clinical Neuropsychiatry*, 8:12–30, 2003.
- [15] A. J. Saykin, H. A. Wishart, T. L. McHugh, et al. IL-6 allelic variation and medial temporal morphology in MCI and older adults with cognitive complaints. In *Alzheimer's Association Int. Conf. on Prevention of Dementia: Early diagnosis and intervention*, Washington, D.C., June 18–21, 2005.
- [16] A. J. Saykin, H. A. Wishart, L. A. Rabin, et al. Older adults with cognitive complaints show brain atrophy similar to that of amnesic MCI. *Neurology*, 67:834–842, 2006.
- [17] L. Shen, H. Huang, F. Makdeon, and A. J. Saykin. Efficient registration of 3d spharm surfaces. In *CRV 2007: Fourth Canadian Conference on Computer and Robot Vision*, pages 81–88, Montreal, QC, May 28–30, 2007.
- [18] L. Shen, A. Saykin, M. K. Chung, and others. Morphometric analysis of genetic variation in hippocampal shape in mild cognitive impairment: Role of an IL-6 promoter polymorphism. In *CSB 2006: LSS Computational Systems Bioinformatics Conf. (Poster)*, Stanford, CA, Aug. 14–18, 2006.
- [19] L. Shen, A. Saykin, T. McHugh, et al. Morphometric MRI study of hippocampal shape in MCI using spherical harmonics. In *Alzheimer's Association Int. Conf. on Prevention of Dementia: Early diagnosis and intervention*, page 120, Washington, D.C., June 18–21, 2005.
- [20] H. A. Wishart, A. J. Saykin, T. W. McAllister, et al. Regional brain atrophy in cognitively intact adults with a single apoe e4 allele. *Neurology*, 67:1221–4, 2006.
- [21] K. Worsley, S. Marrett, P. Neelin, A. Vandal, K. Friston, and A. Evans. A unified statistical approach for determining significant signals in images of cerebral activation. *Human Brain Mapping*, 4:58–73, 1996.